

Article

Study of New Infrared Non-Linear Optical Crystal BaGa₄Se₇ Based on First Principle

Xie Huang ^{1,†}, Rong Dai ^{2,†}, Lei Zhang ², Jing Ning ², Fuchun Zhang ^{2,*} and Junfeng Yan ^{3,*}¹ Network Information Center, Yan'an University, Yan'an 716000, China; hx@yau.edu.cn² School of Physics and Electronic Information, Yan'an University, Yan'an 716000, China; dairong@yau.edu.cn (R.D.); zhanglei@yau.edu.cn (L.Z.); ningjing@yau.edu.cn (J.N.)³ School of Information Science Technology, Northwest University, Xi'an 710127, China

* Correspondence: yadxzfc@yau.edu.cn (F.Z.); yanjf@nwu.edu.cn (J.Y.); Tel.: +86-1832-991-8036 (F.Z.); +86-1362-928-0982 (J.Y.)

† These authors contributed equally to this work.

Abstract: The electronic structure and optical properties of BaGa₄Se₇ crystals were studied by generalized gradient approximation (GGA) and Heyd–Scuseria–Ernzerhof (HSE). The electronic structure results showed that BaGa₄Se₇ is a nonlinear optical crystal with a direct wide band gap. The band gap was calculated to be 2.36 eV using the HSE06 method, which is basically equal to the experimental value. The band structure showed that the top of the valence band was largely contributed by Ga 4s, 4p and Se 4p states, while the bottom of the conduction band was mainly comprised of Ga 4s, 4p, Se 4p, and Ba 5d states. The optical properties showed strong absorption and reflection in the ultraviolet region and strong transmittance in the infrared region. The average static refractive index of BaGa₄Se₇ was 2.73, and the static birefractive index was 0.04. These values indicate that the material has a good phase-matching ability and a wide laser damage threshold. The above results indicate that BaGa₄Se₇ is a potential infrared nonlinear optical crystal material.

Keywords: BaGa₄Se₇; nonlinear optical crystal; optical properties; electronic structure



Citation: Huang, X.; Dai, R.; Zhang, L.; Ning, J.; Zhang, F.; Yan, J. Study of New Infrared Non-Linear Optical Crystal BaGa₄Se₇ Based on First Principle. *Crystals* **2022**, *12*, 143. <https://doi.org/10.3390/cryst12020143>

Academic Editors: Yuri Kivshar and Marco Bazzan

Received: 19 November 2021

Accepted: 15 January 2022

Published: 20 January 2022

Publisher's Note: MDPI stays neutral with regard to jurisdictional claims in published maps and institutional affiliations.



Copyright: © 2022 by the authors. Licensee MDPI, Basel, Switzerland. This article is an open access article distributed under the terms and conditions of the Creative Commons Attribution (CC BY) license (<https://creativecommons.org/licenses/by/4.0/>).

1. Introduction

Chalcogenides compounds have become the main research and application materials in the field of nonlinear infrared crystal materials due to their large nonlinear optical coefficients, suitable birefringence and sufficiently high laser damage thresholds [1–4]. However, the characteristics of metal sulfide in the material's light absorption and the construction of high nonlinear optical effect units make it a new type of mid-to-far infrared nonlinear optical material [5].

BaGa₄S₇ and BaGa₄Se₇ show great second-harmonic generation (SHG) effect in chalcogenides when detected in laser pump, which is about 2–3 times that of the benchmark material AgGaS₂ [6]. This has attracted the wide attention of researchers. Eisenmann [7] et al. reported the Pmn21 space group structure of the BaGa₄S₇ orthorhombic system. Badikov [8,9] and others have successfully grown a high-quality BaGa₄S₇ single crystal, and tested and calculated the phase matching of its refractive index and frequency doubling. However, due to the high melting point of BaGa₄S₇, the difficulty of crystal growth and the low nonlinear coefficient, researchers have found a BaGa₄Se₇ crystal with a larger nonlinear coefficient, a more compact and stable structure [10]. Yao [11] et al. synthesized the BaGa₄Se₇ compound with $\beta = 121.24$ for the first time, and calculated the electronic and optical properties of BaGa₄Se₇ through first principles. The results show that BaGa₄Se₇ is a new type of infrared NLO material with good overall performance and may be practically applied in the future. Yelisseyev [12] and others subsequently grew a large BaGa₄Se₇ crystal, and used crystal optics and spectroscopy to study its optical properties, proving the possibility of controlling the luminescence parameters by annealing after growth in a

suitable atmosphere. The non-centrosymmetric structure of the crystal is confirmed, and the experimental results show that BaGa₄Se₇ is used as an infrared NLO material in many practical applications. Kolker [13] et al. report on the first BaGa₄Se₇ nanosecond optical parametric oscillator pumped by Q-switched Nd:YLiF₄ laser at 1053 nm. The research results show that this newly discovered biaxial monoclinic chalcogenide compound can effectively realize mid-infrared nonlinear down-conversion within its full transparency range (0.47–18 μm) and has good application prospects. However, a more comprehensive evaluation of the performance of BaGa₄Se₇ crystals requires more accurate calculations for support.

In this work, the electronic and optical properties of the BaGa₄Se₇ crystal are calculated by the first-principles method. GGA [14] and HSE [15] are used to calculate the electronic properties of the crystal, such as the energy band, density of states, and charge density difference. The optical properties such as static birefringence, transmittance, absorption and reflection characteristics of the crystal are systematically analyzed. The effects of various factors on the performance of BaGa₄Se₇ crystals are studied.

2. Theoretical Model and Computational Method

2.1. Theoretical Model

BaGa₄Se₇ has a geometric structure similar to that of BaGa₄S₇ [16]. The unit cell parameters are as follows: cell parameter $a = 7.739 \text{ \AA}$, $b = 6.635 \text{ \AA}$, $c = 14.936 \text{ \AA}$, $\alpha = \gamma = 90^\circ$, $\beta = 121.048^\circ$, unit cell volume 766.937 \AA^3 . The structure model used in the calculation is shown in Figure 1. The GaSe₄ tetrahedrons are connected with the vertices to form a three-dimensional frame structure. Ba atoms are located in the frame air attack, and each Ba atom is coordinated with 8 Se atoms. Compared with BaGa₄S₇, BaGa₄Se₇ has a more compact and stable structure.

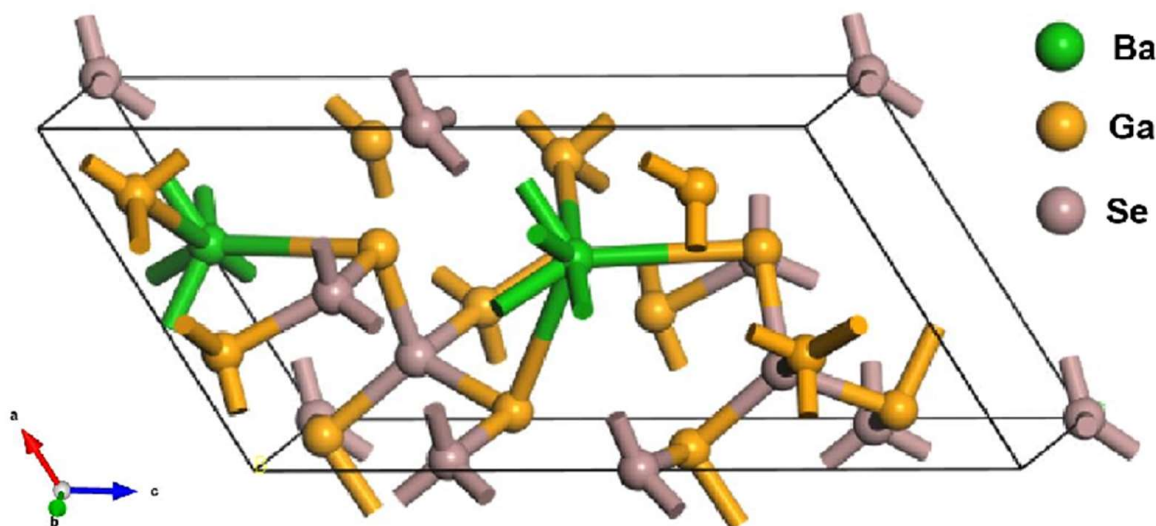


Figure 1. The structural model of BaGa₄Se₇.

2.2. Computational Details

All theoretical investigations were performed via the Vienna Ab initio Simulation Package code (VASP) [17]. Geometry optimizations were conducted using the highly accurate GGA method with the Perdew–Burke–Ernzerhof (PBE) exchange–correlation function [18]. The precision of energy convergence was $1 \times 10^{-6} \text{ eV}$, while the force between atoms was 0.01 eV/\AA , and the maximum displacement accuracy between atoms was $5 \times 10^{-6} \text{ eV}$. The cut-off energy of the plane wave was set to 560 eV. The first Brillouin zone was sampled with a $3 \times 3 \times 2$ k-point grid, the energy convergence accuracy was $5.0 \times 10^{-6} \text{ eV}$, and the total interatomic force was 0.01 eV/\AA . The highly accurate GGA and

the hybrid density function of HSE [19] was applied to the calculations to obtain accurate electronic structures and optical characteristics theoretically.

3. Results and Discussion

3.1. Geometric Properties

The structure of the BaGa₄Se₇ crystal was optimized by the BFGS method, the optimized results and the experimental results are shown in Table 1. The theoretically calculated BaGa₄Se₇ lattice constants were $a = 7.739 \text{ \AA}$, $b = 6.635 \text{ \AA}$, $c = 14.936 \text{ \AA}$, $\alpha = \gamma = 90$, $\beta = 121.048$, and the BaGa₄Se₇ crystal belongs to the orthorhombic crystal system, while the experimentally achieved results were $a = 7.625 \text{ \AA}$, $b = 6.511 \text{ \AA}$, $c = 14.702 \text{ \AA}$, $\alpha = \gamma = 90$, $\beta = 121.240$, and the relative error was not more than 0.019. The theoretical values are consistent with the experimental values. The results show that the accuracy and reliability of the theoretical model and calculation parameters of BGS material are stable.

Table 1. Comparison of geometric structure optimization results and experimental results of BGS.

Parameters	Theoretical Value	Experimental Value [11]	Relative Errors
$a/\text{\AA}$	7.739	7.625	0.014
$b/\text{\AA}$	6.635	6.511	0.019
$c/\text{\AA}$	14.936	14.702	0.015
$\alpha = \gamma(^{\circ})$	90	90	0.000
$\beta(^{\circ})$	121.048	121.240	0.001

3.2. Electronic Structure

3.2.1. Band Structure and Density of States

Based on first principles, the band structure and density of states of BaGa₄Se₇ crystals were systematically studied by GGA and hybrid functional (HSE06, HSE03, B3LYP and PBE0) methods. The theoretical results obtained by the two methods were compared. Figure 2 shows the band structure of BaGa₄Se₇ calculated by GGA and hybrid functional methods, and the Fermi level E_f was 0 eV. The top and bottom of the valence band obtained by the two methods are located at the Γ point, indicating that BaGa₄Se₇ belongs to the direct band gap semiconductor material. The valence band energy portion may be divided into four regions. The valence band region near the Fermi surface overlaps. The band gaps calculated by the GGA, HSE06, HSE03, B3LYP and PBE0 [14,15,18] methods are 1.603 eV, 2.360 eV, 2.396 eV, 2.844 eV and 3.013 eV, respectively. Since the calculated value of the GGA method is usually estimated to be smaller than its true value, the value calculated by the hybrid functional method is usually used for analysis. The energy at the top of the valence band calculated by the two methods is smoother than the energy at the bottom of the conduction band. This indicates that the bottom of the electron effective mass of the conduction band is smaller than the mass of the top of the valence band hole. The conduction band electrons show high mobility. The holes in the valence band show low mobility and the top of the valence band are non-local, and the atomic orbitals that make up the energy band are highly expandable [20]. The laser damage threshold of crystals is particularly important in high-power laser applications. Under the action of the laser, the power limit that optical components can withstand is closely related to the bandgap value of the crystal. The larger the band gap value, the higher the laser damage threshold. As shown in Table 2, the valence band calculated by HSE03 showed a maximum at G, and the conduction band showed a minimum at this point, which indicates that BaGa₄Se₇ is a direct band gap semiconductor. Table 3 lists the bandgaps of BaGa₄Se₇ by GGA and hybrid functional methods.

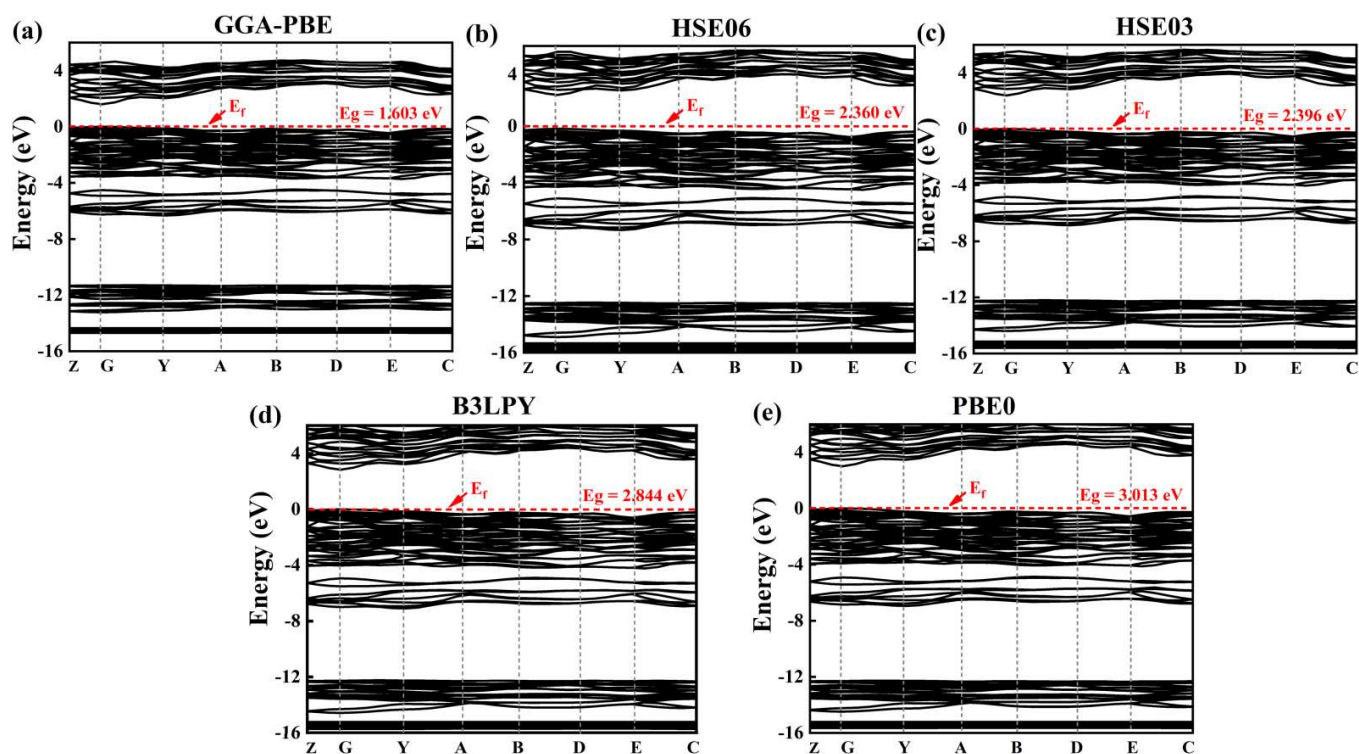


Figure 2. Band structure of BaGa₄Se₇. (a) GGA method, (b) HSE06 method, (c) GGA method, (d) HSE06 method. (e) PBE0 method.

Table 2. The characteristic energy values at E_V and E_C of the first Brillouin region of BaGa₄Se₇.

Method	Parameter	Z	G	Y	A	B	D	E	C
GGA	E_V (eV)	−0.084	0	−0.125	−0.256	−0.197	−0.258	−0.449	−0.170
	E_C (eV)	2.070	1.600	2.050	2.840	3	3.100	2.920	2.370
HSE06	E_V (eV)	−0.084	0	−0.198	−0.368	−0.237	−0.294	−0.540	−0.251
	E_C (eV)	2.942	2.360	2.860	3.711	3.849	3.960	3.850	3.201
HSE03	E_V (eV)	−0.086	0	−0.203	−0.378	−0.241	−0.297	−0.528	−0.242
	E_C (eV)	2.960	2.396	2.840	3.660	3.850	3.940	3.760	3.170
B3LYP	E_V (eV)	0.098	0	−0.151	−0.374	−0.277	−0.359	−0.600	−0.212
	E_C (eV)	3.310	2.840	3.240	4.140	4.250	4.410	4.220	1.360
PBE0	E_V (eV)	−0.094	0	−0.217	−0.409	−0.263	−0.314	−0.560	−0.260
	E_C (eV)	3.500	3.010	3.470	4.310	4.510	4.600	4.420	3.820

Table 3. The bandgap of BaGa₄Se₇ by GGA and hybrid functional methods.

Method	Theoretical Value (eV)	Experimental Value (eV)	Relative Error /%
GGA	1.603	2.640	0.392
HSE03	2.396	2.640	0.092
HSE06	2.360	2.640	0.106
B3LYP	2.844	2.640	0.080
PBE0	3.013	2.640	0.141

Figure 3 is the calculation of the total density of states and partial density of states of BaGa₄Se₇ using the GGA and hybrid functional methods, reflecting the contribution of different electronic states to the valence band and conduction band. The projected density of states shows the contribution of each atomic orbital. It can be seen from Figure 3 that the s orbital is mainly provided by Ga and Se atoms, the p orbital is mainly provided by Ba, Ga and Se atoms, and the d orbital is mainly provided by Ba and Ga atoms. Simultaneously,

Figure 3a shows that the valence band is composed of four energy regions, $-29\sim-26$ eV, $-18\sim-13$ eV, $-13\sim-10$ eV, $-8\sim 0$ eV, two different pans. The shape of the density of states calculated by the function is similar, and the peak position has a certain shift. In the conduction band, the position of the density of state peak calculated by HSE06 moves to the high energy region, and the valence band near the Fermi surface basically coincide. At the low energy region of the valence band, the position of the density of state peak calculated by HSE06 moves to the low energy direction. The $-28\sim-26$ eV Valence zone (HSE06 was $-39\sim-28$ eV) is contributed by Ba-s orbital electrons, this orbital Ba atom does not form chemical bonds with other atoms; $-15\sim-13$ eV valence zone (HSE06 is $-18\sim-15$ eV) contributed by Ga atom $3d$ orbital and Se $4s$ orbital electrons, Ga $3d$ orbital.

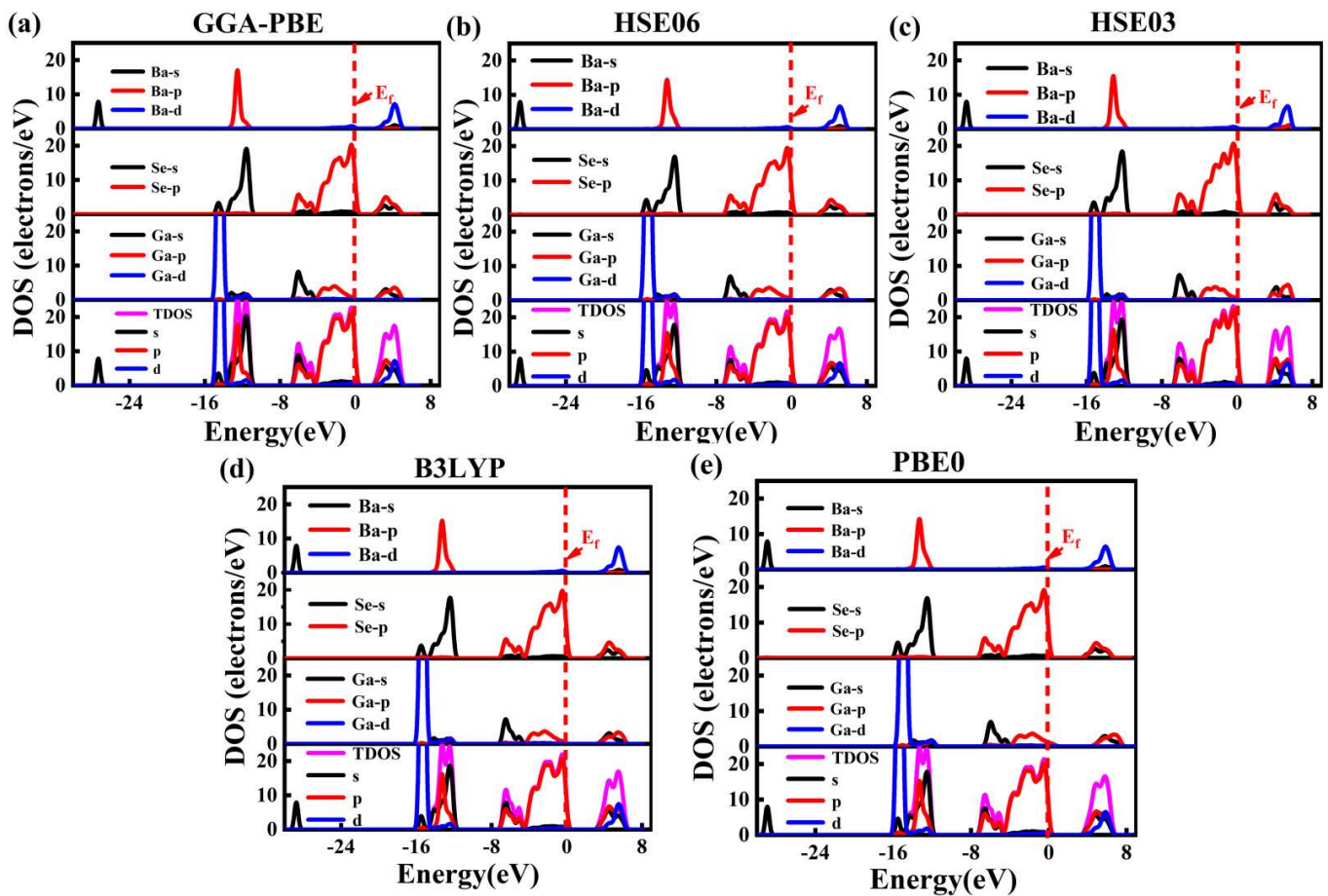


Figure 3. The global state density and partial wave state density of BaGa₄Se₇, (a) GGA method, (b) HSE06 method, (c) HSE03 method, (d) B3LYP method and (e) PBE0 method.

Electrons have a greater contribution, and have a certain contribution to the Ga and Se chemical bond; the $-13\sim-10$ eV valence band region (HSE06 was $-15\sim-12$ eV) Ba $5p$ orbital and Se $4s$ orbital have a certain contribution to the chemical bond of Ba and Se; the valence band region of $-8\sim 0$ eV is mainly composed of Ga $4s$ and $4p$, Se $4p$, orbital electrons, showing Ga and Se atoms The orbital hybridization between Ga and Se atoms indicates that there is a strong chemical bond between Ga and Se atoms. The main contribution from the bottom of the conduction band by Ga $4s$, $4p$, Se $4p$, and Ba $5d$ orbital electrons, indicating that $[\text{Ga}_4\text{Se}_7]^{-2}$ determines the energy band gap of BaGa₄Se₇ shows that the optical properties of BaGa₄Se₇ are mainly determined by the electron orbital coupling between Ga and Se atoms. The orbital electrons of Ba have a strong locality and make little contribution to optical properties.

3.2.2. Differential Charge Density

Figure 4 shows a graph of the differential charge density of BaGa_4Se_7 . In Figure 4a, the green area indicates the loss of electrons, and the yellow area indicates the gain of electrons. The differential charge density of the unit cell can more intuitively understand the bonding characteristics and electron transfer between BaGa_4Se_7 atoms. It can be seen from the figure that Se atoms have a strong ability to gain electrons, Ga atoms have a strong ability to lose electrons, Ba atoms are relatively isolated, and the ability to lose electrons is weak. Se-Ga atoms form strong chemical bonds, and Ba and Se atoms form relatively weak chemical bonds. Figure 4b shows the differential charge density diagram of BaGa_4Se_7 . The blue area represents the electronic loss, and the red area represents the electronic gain. The depth of the color is related to the number of transferred electrons, the darker the color change, the more electrons transferred. It can be seen from the figure that the electron cloud distribution between Ga atoms and Se atoms is anisotropic, and the electron cloud around the Se atoms has strong polarization characteristics. In addition, the electron cloud density between Ga atoms and Se atoms overlaps to a certain extent, and the electron clouds outside the Ga nucleus are all segregated toward the Se atoms. From the electronegativity of the atoms, Ga atoms have a strong ability to lose electrons, and Se atoms can gain electrons. The positive and negative charge centers do not overlap, and a strong polar covalent bond is formed between the two atoms, while the Ba atom is quite ionized and isolated, with a very small amount of overlap with the electron cloud density between the Se atoms, and the charge distribution is close. It is spherical, so Ga, Se, and Ba atoms exhibit strong ionic bond characteristics, and the covalent bond is weak. These results indicate that BaGa_4Se_7 has weak and strong covalent bonds mixing with an ionic semiconductor material.

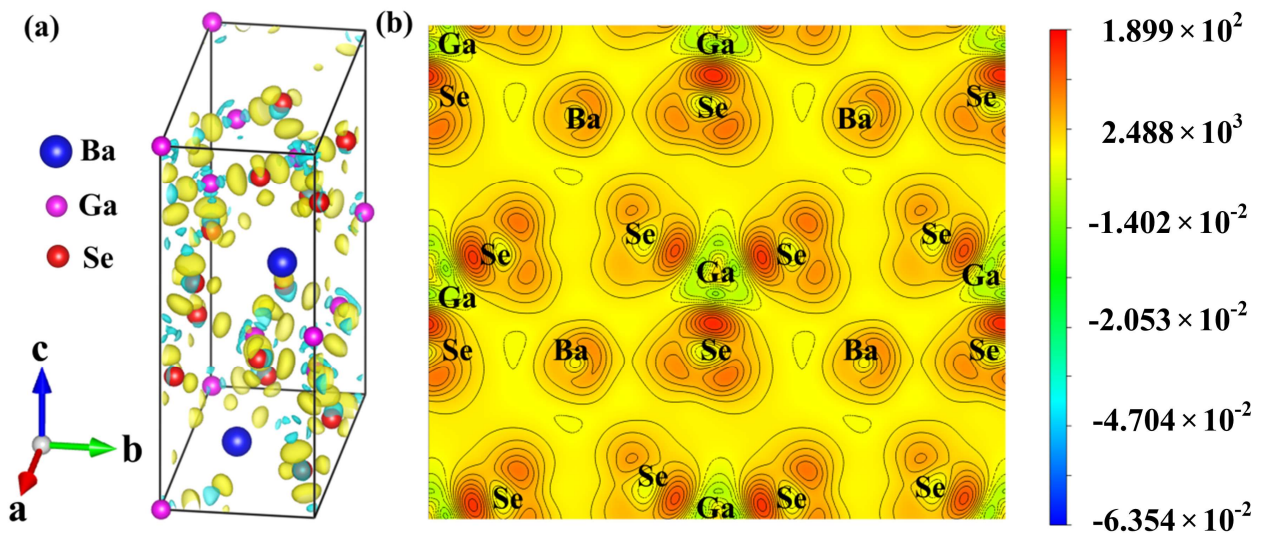


Figure 4. (a) Three-dimensional diagram of differential charge density of BaGa_4Se_7 , (b) the differential charge density diagram of BaGa_4Se_7 .

3.3. Optical Properties

The macroscopic optical properties of solids can be described by complex dielectric function or complex refractive index in the linear response range

$$\varepsilon_1 = n^2 - \kappa^2 \quad (1)$$

$$\varepsilon_2 = 2n\kappa \quad (2)$$

where n and κ are the refractive index and extinction coefficient, respectively.

Usually using adiabatic approximation and single electron approximation to discuss the interaction between light and solid, while indirect transitions are ignored, and only

the excitation of electrons in direct transitions is considered. According to the definition of the direct transition probability and the Kramers–Kronig dispersion relationship, the energy loss of reflectance, absorption coefficient, complex refractive index, birefringence and crystal dielectric function can be obtained [21–23]

$$\varepsilon_2(\omega) = \frac{\pi}{\varepsilon_0} \left(\frac{e}{m\omega} \right)^2 \cdot \sum_{V,C} \left\{ \int_{BZ} \frac{2d\vec{K}}{(2\pi)^3} \left| \vec{a} \cdot \vec{M}_{V,C} \right|^2 \delta[E_C(\vec{K}) - E_V(\vec{K}) - \hbar\omega] \right\} \quad (3)$$

$$\varepsilon_1(\omega) = \mathbf{1} + \frac{2e}{\varepsilon_0 m^2} \cdot \sum_{V,C} \int_{BZ} \frac{2d\vec{K}}{(2\pi)^3} \frac{\left| \vec{a} \cdot \vec{M}_{V,C}(\vec{K}) \right|^2}{\left[E_C(\vec{K}) - E_V(\vec{K}) \right] / \hbar} \cdot \frac{1}{\left[E_C(\vec{K}) - E_V(\vec{K}) \right]^2 / \hbar^2 - \omega^2} \quad (4)$$

$$R(\omega) = \frac{(n-1)^2 + k^2}{(n+1)^2 + k^2} \quad (5)$$

$$\alpha \equiv \frac{2\omega\kappa}{c} = \frac{4\pi\kappa}{\lambda_0} \quad (6)$$

$$L(\omega) = \text{Im} \left(\frac{-1}{\varepsilon(\omega)} \right) = \frac{\varepsilon_2(\omega)}{[\varepsilon_1^2(\omega) + \varepsilon_2^2(\omega)]} \quad (7)$$

where ε_0 is the dielectric constant in a vacuum, λ_0 is the wavelength in vacuum, \hbar is Planck constant, C and V are conduction and valence bands, BZ is the first Brillouin zone, \vec{K} is electron wave vector, \vec{a} is the unit direction vector of vector potential A, $M_{V,C}$ is the transition matrix element, ω is the frequency of the electromagnetic wave, $E_C(\vec{K})$ and $E_V(\vec{K})$ are the eigenlevels on the conduction and valence bands, $R(\omega)$ is the reflectivity, α is the absorption coefficient and $L(\omega)$ is the energy loss function.

3.3.1. BaGa₄Se₇ Complex Dielectric Function

The dielectric function is mainly used to characterize all kinds of spectral information of the crystal, reflecting the energy band structure and electronic structure of the material. As a semiconductor material, the BaGa₄Se₇ spectrum by electronic transitions between energy levels is generated, the peak of each dielectric can be explained by the band structure and the density of states of the material.

As was already mentioned, BaGa₄Se₇ belongs to the orthorhombic crystal system, so in order to study the optical anisotropy of the crystal, the incident light of which the polarization direction was in parallel to the crystal axis was selected. Figure 5a,b shows the real part of the dielectric function ε_{1x} , ε_{1y} , ε_{1z} calculated by GGA and HSE06 methods, and Figure 5c,d shows the imaginary part ε_{2x} , ε_{2y} , ε_{2z} × z obtained by GGA and HSE06 methods. As shown in Figure 5, the curve shape of the real parts of the dielectric function calculated by the two methods was similar, while the peak value was not at the same photon energy and was not equal. By comparing Figure 5a,b, it can be seen that the maximum value of the dielectric function calculated by the GGA method was 9.32 and located at 2.76 eV, while the maximum value of the dielectric function calculated by the HSE06 method was 6.28 and located at 4.36 eV. When the frequency of $\varepsilon_1(\omega)$ was 0, the average static dielectric constant $\varepsilon_1^{ave}(0)$ of BaGa₄Se₇ calculated by GGA and HSE06 methods were 5.906 and 3.74, respectively. However, the average static dielectric constants $\varepsilon_1(\omega)$ coincided with each other in different directions, and the peak was also in the same position. All the above facts showed that the optical anisotropy of BaGa₄Se₇ crystal is relatively weak [24]. In the next step, we further investigated the reflectivity, absorption coefficient, complex refractive index, birefringence, and loss function.

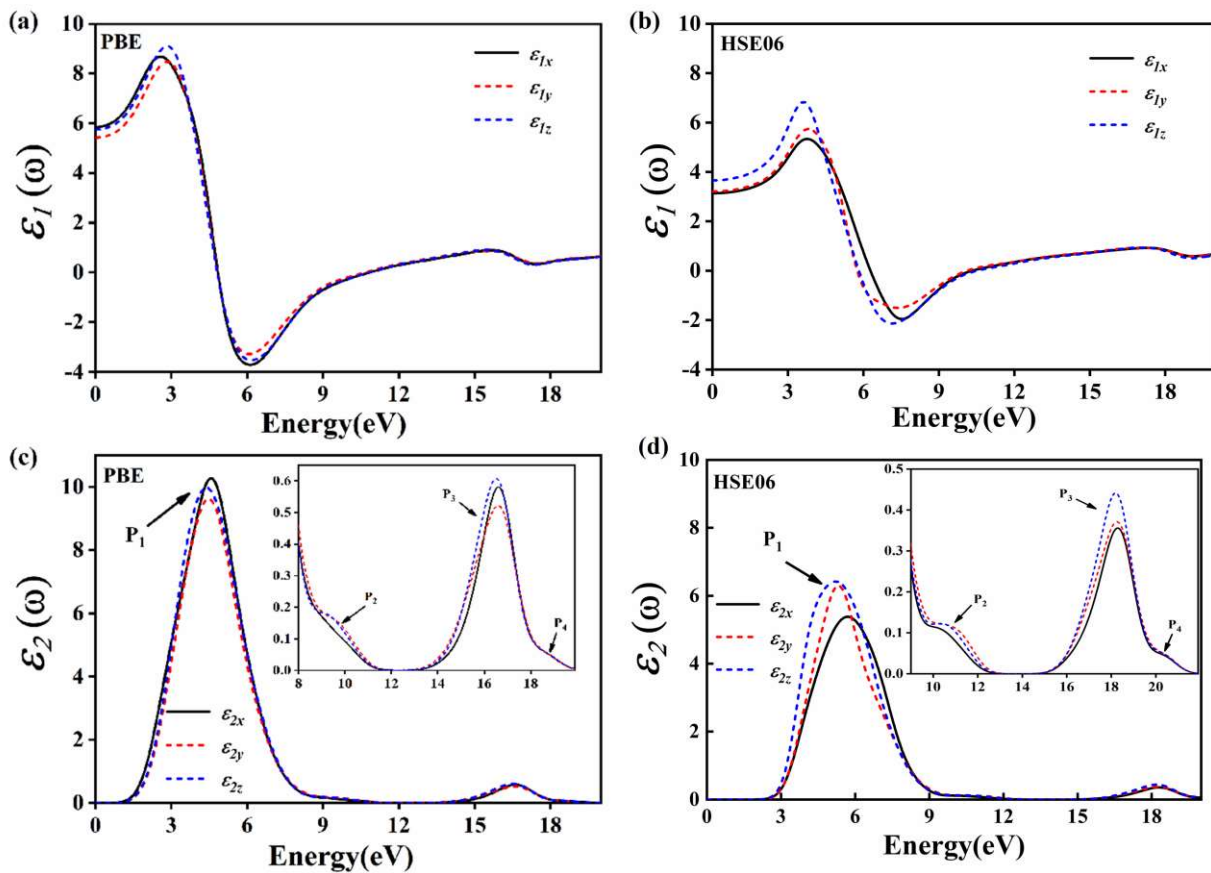


Figure 5. Complex dielectric function of BaGa₄Se₇; the real part of the dielectric function calculation of GGA (a) and HSE06 (b) method, the imaginary part of the dielectric function calculation of GGA (c) and HSE06 (d) method.

The imaginary part of the complex dielectric function $\varepsilon_2(\omega)$ determines the linear response of the light field [25,26]. The results in Figure 5c show a method in GGA, corresponding to the bottom of the conduction band electron transitions directly associated with the threshold of transition from the valence band to the top of the peak at 1.07 eV at the dielectric. The first $\varepsilon_2(\omega)$ peak was located at 4.65 eV, which was mainly due to the valence band from the conduction band of the electron transitions, so the $\varepsilon_2(\omega)$ gradually tended to decrease with the increase of photon energy. When the photon energy was less than 18.0 eV, there were four peak values of P₁, P₂, P₃, and P₄ in the imaginary part of the dielectric function, and the corresponding photon energies were 4.45 eV, 9.18 eV, 16.21 eV, and 18.84 eV, respectively. From the HSE06 calculation results (Figure 5d), the first $\varepsilon_2(\omega)$ peak was located at 5.88 eV, which could be assigned to the electron transition from the upper valence band to the bottom of the conduction band. When the photon energy was lower than 21 eV, the imaginary part of the dielectric function also had four dielectric electrode peaks with photon energies at 5.88 eV, 10.78 eV, 18.11 eV, and 20.34 eV, respectively. As the photon energy increased, $\varepsilon_2(\omega)$ gradually decreased, and finally tended to 0. For the P₁ peak, it was known from the density of states diagram that it could be mainly derived from the transition of the p-state electrons of O and Ga atoms to the bottom of the conduction band. The P₂ peak was derived from the transition of the s-state electrons of Se and Ga atoms to the bottom of the conduction band. Furthermore, the P₃ peak could be assigned to the transition of the Se electron of the Se atom to the bottom of the conduction band, while the P₄ peak could be originated from the transition of the d state of the Ga atom and the p state of the Ba atom to the bottom of the conduction band. These dielectric peaks corresponded to the reflection peaks given in the reflection spectrum (Figure 6), which were the macroscopic manifestation of the interband transition of the electrons of solid under

the perturbation of the photoelectromagnetic wave field. In other words, the transition mechanism of the reflection peak was consistent with that of the absorption peak of the dielectric spectrum.

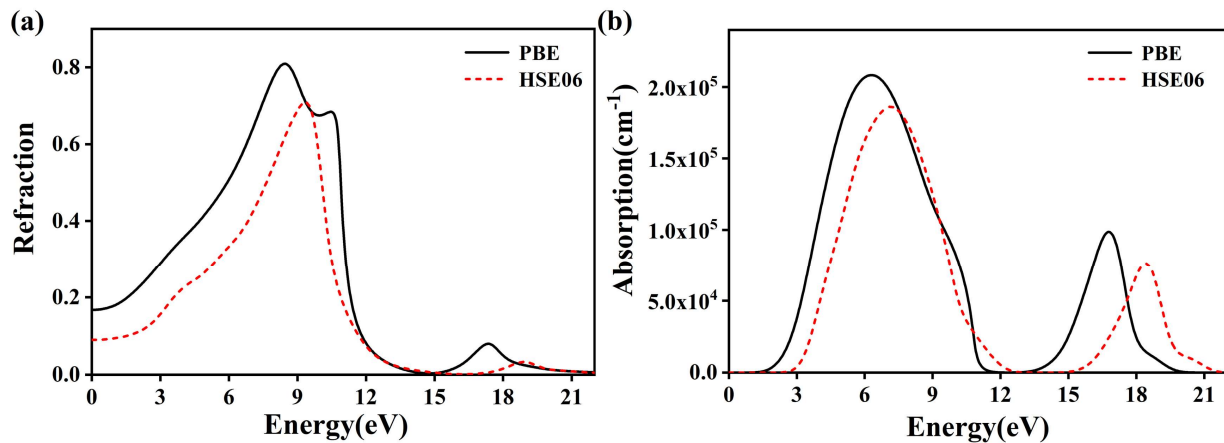


Figure 6. The reflection spectrum and absorption spectrum of BaGa₄Se₇, (a) the reflection spectrum, (b) the absorption spectrum.

3.3.2. BaGa₄Se₇ Reflection and Absorption Spectrum

Figure 6 shows the reflection and absorption spectra of the BaGa₄Se₇ crystals calculated by GGA and HSE06. Figure 6a shows the reflection spectrum of BaGa₄Se₇. The calculation results of GGA and HSE06 showed that the shape of the reflection spectrum calculated by the two methods was very similar, the energy was less than 10.65 eV, and the reflectance calculated by the HSE06 method was significantly larger, the energy was equal to 10.65 eV, and the reflectance was the same. When the energy was less than 4 eV, the reflectance calculated by GGA was less than 16%, and the reflectance calculated by HSE06 was less than 29%. Then, the reflectance increased with the increase of energy, which is due to the influence of the energy band transition of BaGa₄Se₇. The energy was near 8.77 eV, and the reflectivity reached the peak value. The GGA result was 80.5%, and the HSE06 result was 64.6%. As the energy continued to increase, the reflectivity rapidly decreased to zero. When the energy exceeded 21 eV, the optical opacity was displayed. The above results show that the BaGa₄Se₇ crystal has a strong reflection in the ultraviolet band, low reflectivity in the infrared band, and strong corresponding light transmittance. Figure 6b shows the absorption spectrum of BaGa₄Se₇, with an absorption coefficient of 10⁵ cm⁻¹. The optical absorption is the most important optical property. The BaGa₄Se₇ crystal reflects light emission spectrum of the mechanism by the electronic transitions between the energy levels produced. The shape of the absorption spectrum calculated by the two methods is also very similar. The absorption edge calculated by GGA was at 1.804 eV, and the absorption edge calculated by HSE06 was at 2.918 eV, which falls in the ultraviolet region. This is related to the bandgap value. Intrinsic absorption begins to appear on the absorption edge. As the photon energy increases (the wavelength decreases), the absorption coefficient increases sharply by the order of 10⁵, and strong light absorption occurs, indicating the start of a direct transition. GGA calculated the strongest absorption peak at 5.78 eV, corresponding to the wavelength of 204 nm, HSE06 calculated the strongest absorption peak at 7.76 eV, the corresponding wavelength was 225 nm, located in the ultraviolet region, the corresponding transmittance was small, in contrast, to absorption in the infrared band. The coefficient was very small, and the corresponding transmittance was relatively large. According to the above analysis results of the reflection spectrum and absorption spectrum, it can be seen that the BaGa₄Se₇ crystal has a higher reflectivity and absorption coefficient in the ultraviolet band, and a lower reflectivity and absorption coefficient in the infrared band, corresponding to stronger transmittance, and the larger band gap value. The larger range of the light-transmitting area and the bandgap value calculated according to the HSE06

method was 2.58 eV, it can be seen that the shortest wavelength of the transmitted light was about 0.30 μm . The area can be used as an important frequency conversion crystal.

3.3.3. BaGa₄Se₇ Complex Refractive Index

Figure 7 is the calculated complex refractive index of the BaGa₄Se₇ tetragonal crystal. The complex refractive index is the most important optical constant of the absorbing medium. The real refractive index n is determined by the propagation speed of the light wave in the BaGa₄Se₇ tetragonal crystal, and the imaginary extinction coefficient k is determined by the attenuation (absorption of light energy) when the light wave propagates in the BaGa₄Se₇ tetragonal crystal. From the results in the figure, it can be concluded that the calculation curves of the GGA and HSE06 methods are very similar. The peak is not at the same photon energy. The refractive index calculated by the GGA method was 2.4, and the maximum peak of 3.11 corresponds to the photon energy value of 2.73 eV. When the photon energy is 20 eV, the extinction coefficient is reduced to 0, and the refractive index tends to be flat with frequency, approximately equal to 1, which changes to normal dispersion. Using the HSE06 method to calculate, the refractive index was 1.91, the maximum peak value was 4.61, and the corresponding photon energy value was 2.67 eV. When the photon energy is 21.6 eV, the extinction coefficient decreases to 0, and the refractive index tends to be flat with frequency, changing to normal dispersion.

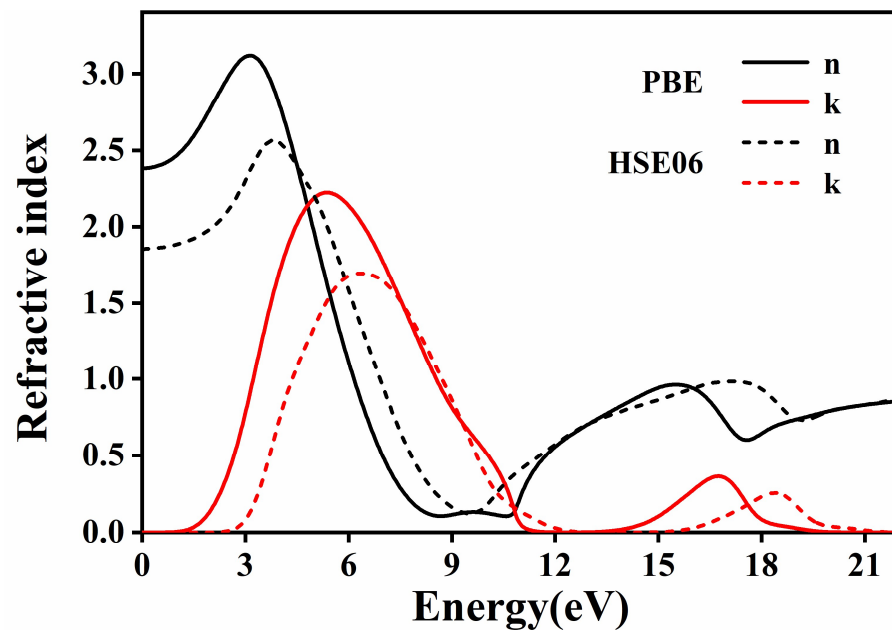


Figure 7. Complex refractive index of BaGa₄Se₇.

3.3.4. BaGa₄Se₇ Refractive Index and Birefringence

Figure 8 shows a graph of the main refractive index and birefringence Δn of BaGa₄Se₇ crystals in different directions calculated by the GGA and HSE06 methods as a function of energy. The average static refractive indexes calculated by GGA and HSE03 methods were 2.27 and 1.88, respectively. The birefringence is defined as the maximum difference Δn between two or three principal refractive indexes in a heterogeneous body, which is an important physical quantity to measure the performance of nonlinear crystals. It can be seen from Figure 8 that the static birefringence of BaGa₄Se₇ calculated by the GGA method was 0.118, which had a maximum value (0.35) at an energy value of 3.06 eV. In the infrared region, its birefringence was less than 0.118. The static birefringence of BaGa₄Se₇ calculated by the HSE06 method was 0.140, which had a maximum value (0.20) at an energy value of 4.75 eV, while in the infrared region, its birefringence was less than 0.140. The results show that, due to the small bandgap of BaGa₄Se₇ tetragonal crystal calculated by the GGA

method, the average static refractive index became larger, and the range of birefringence changed in the mid-to-far infrared region. However, sufficient second-order frequency doubling (second harmonic generation, SHG) and suitable birefringence output are the conditions for judging whether a nonlinear optical crystal material is good. The smaller the refractive index, the more effective it is to avoid the loss of SHG output conversion rate. The average static refractive index of BaGa₄Se₇ is 1.88, which is smaller than the refractive index of the commercially available infrared nonlinear optical crystal, AgGaS₂ [27]. The proper birefringence can not only enable the nonlinear optical crystal to achieve phase matching in a wider band but also avoid the dispersion effect that causes the nonlinear efficiency to decrease. The calculation results show that the BaGa₄Se₇ tetragonal crystal has excellent phase matching performance, and the bandgap value of the BaGa₄Se₇ tetragonal crystal is 2.360 eV. The above conclusions show that BaGa₄Se₇ tetragonal crystal is an excellent infrared nonlinear optical material. This appropriate birefringence rate, high laser damage threshold and wide transmission band range are basic conditions for excellent nonlinear optical crystal performance and are widely used in the field of military infrared confrontation [28], environmental monitoring [29] and medical [30] applications. The resulting optical properties of the material are predicted by theoretical calculations, which is of great help to the experiments.

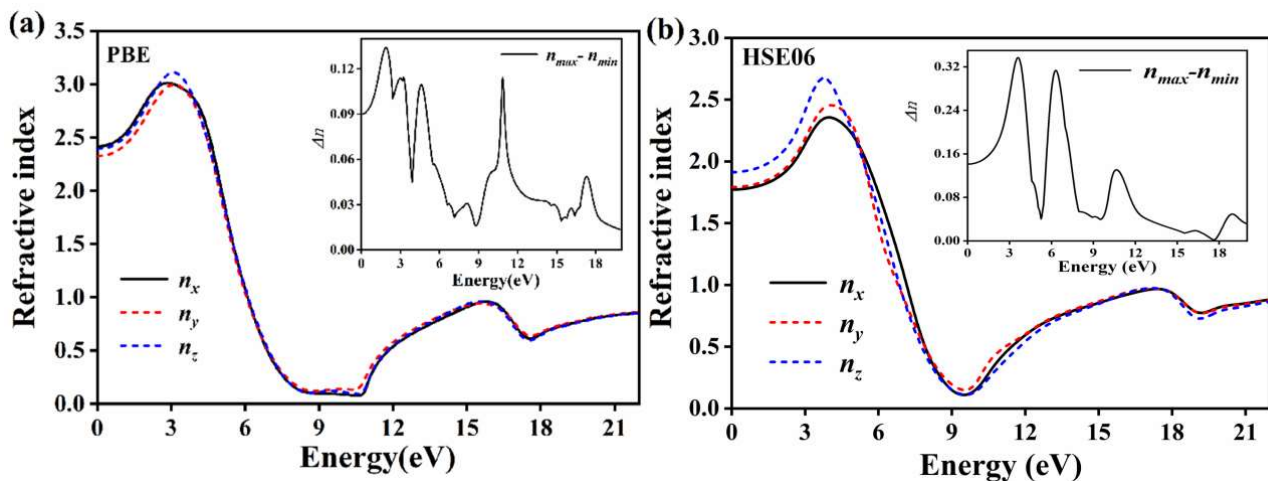


Figure 8. Main index and birefringence of BaGa₄Se₇, (a) GGA method, (b) HSE06 method.

3.3.5. BaGa₄Se₇ Energy Loss Function

Figure 9 shows the energy loss spectrum of the BaGa₄Se₇ tetragonal crystal, describing the loss of energy when electrons pass through a uniform dielectric. It represents the loss function peak plasma oscillation-related features, called the oscillation frequency corresponding to the plasma frequency. It can be seen from the figure that the maximum electron energy loss peaks of the BaGa₄Se₇ tetragonal crystal calculated by the GGA and HSE06 methods located at 10.66 eV and 10.30 eV, and their values were 27.59 and 7.55. This result is consistent with the result of the reflection spectrum in Figure 6a. In addition, from the analysis of the energy band structure diagram in Figure 2 and the density of states diagram in Figure 3, it shows that the peak is derived from the transition from the Ba *s* state to the bottom of the conduction band. The calculation results of the HSE06 method show that when the energy is greater than 21 eV, the electrons of the BaGa₄Se₇ crystal energy loss is zero, which corresponds to the extinction coefficient.

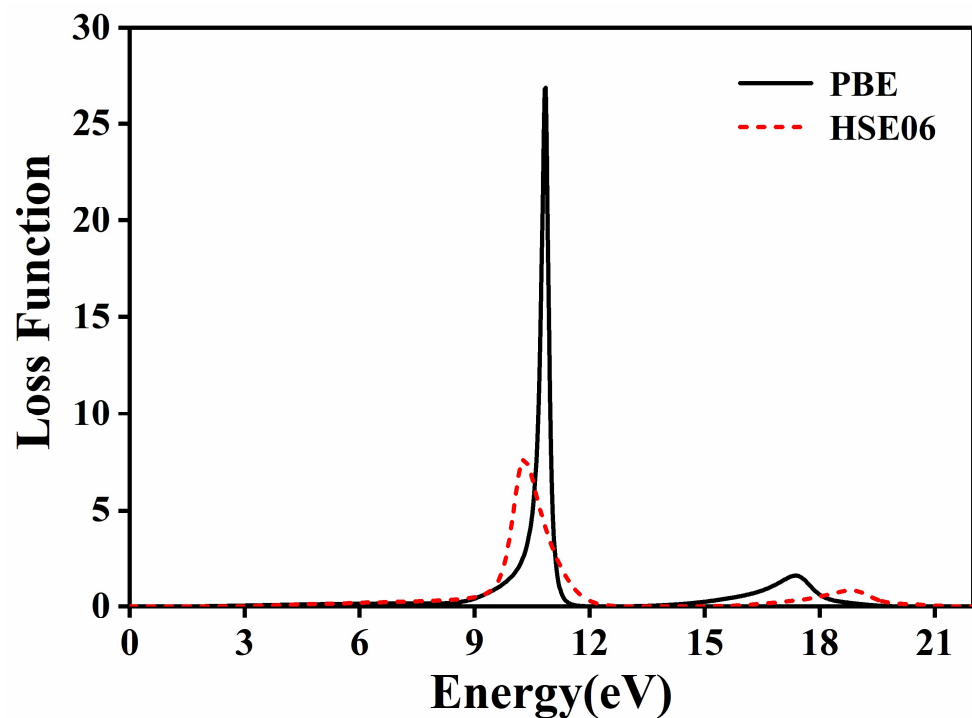


Figure 9. Energy loss function of BaGa₄Se₇.

4. Conclusions

In this work, we used PBE, HSE06, HSE03 B3LYP, and PBE0 methods to calculate the electronic structure and optical properties of BaGa₄Se₇ crystals. By comparing and analyzing the results of the four methods, the band gap values calculated by the HSE06 method were basically consistent with the experimental values, showing that this method is the most suitable for calculating crystal properties. The band structure showed that the top of the valence band was largely contributed by Ga *4s*, *4p* and Se *4p* electrons, while the bottom of the conduction band mainly comprised Ga *4s*, *4p*, Se *4p*, and Ba *5d* electrons. The calculated optical properties show that the BaGa₄Se₇ crystal has strong absorption and reflection characteristics in the ultraviolet region and strong transmittance in the infrared region. These results indicate that the BaGa₄Se₇ crystal is an excellent infrared nonlinear crystal material.

Author Contributions: Conceptualization and experiment, X.H. and R.D.; methodology, F.Z. and J.Y.; validation, L.Z.; data analysis, J.N.; resources, F.Z.; writing—original draft preparation, R.D.; writing—review and editing, R.D. and F.Z. All authors have read and agreed to the published version of the manuscript.

Funding: We acknowledge Kui Gong, Yibin Hu and Yin Wang (all from HZWTECH) for help and discussions regarding this study. This research was funded by [Fuchun Zhang] grant number [61664008], [Fuchun Zhang] grant number [2021]Q-635, [Fuchun Zhang] grant number [2017CXTD-01], [Fuchun Zhang] grant number [S202010719016].

Institutional Review Board Statement: Not applicable.

Informed Consent Statement: Not applicable.

Data Availability Statement: Not applicable.

Conflicts of Interest: The authors declare no conflict of interest.

References

1. Boyd, G.D.; Kasper, H.M.; Mcfee, J.H. Linear and nonlinear optical properties of some ternary selenides. *IEEE J. Quantum Electron.* **1972**, *8*, 900–908. [\[CrossRef\]](#)
2. Wagner, S.; Shay, J.L.; Migliorato, P.; Kasper, H.M. CuInSe₂/CdS heterojunction photovoltaic detectors. *Appl. Phys. Lett.* **1974**, *25*, 434. [\[CrossRef\]](#)
3. Burland, D.M.; Miller, R.D.; Walsh, C.A. Second-order nonlinearity in poled polymer systems. *Chem. Rev.* **1994**, *94*, 31–75. [\[CrossRef\]](#)
4. Zhang, G.D.; Wang, S.P.; Tao, X.T. Research Progress of Infrared Nonlinear Optical Crystals. *J. Synth. Cryst.* **2012**, *41*, 7–17.
5. Havva, B.O.; Haci, O.; Engin, D. A new quaternary semiconductor compound (Ba₂Sb₄GeS₁₀): Ab initio study. *Philos. Mag.* **2017**, *97*, 549–560.
6. Yao, J.Y.; Yin, W.L.; Feng, K. Growth and characterization of BaGa₄Se₇ crystal. *J. Cryst. Growth* **2012**, *346*, 1–4. [\[CrossRef\]](#)
7. Eisenmann, B.; Jakowski, M.; Schafer, H. Zur Kenntnis BaAl₄S₇ and BaGa₄S₇. *Rev. Chim. Miner.* **1983**, *20*, 329–337.
8. Badikov, V.; Badikov, D.; Shevyrdyaeva, G. BaGa₄S₇: Wide-bandgap phase-matchable nonlinear crystal for the mid-infrared. *J. Opt. Soc. Am.* **2011**, *190*, 4330–4410.
9. Badikov, V.; Badikov, D.; Shevyrdyaeva, G. Phase-matching properties of BaGa₄S₇ and BaGa₄Se₇. wide-bandgap nonlinear crystals for the mid-infrared. *Phy. Stat. Sol.* **2011**, *5*, 3103.
10. Zhai, N.; Li, C.; Xu, B.; Bai, L.; Yao, J.; Zhang, G.; Hu, Z.; Wu, Y. Temperature-Dependent Sellmeier Equations of IR Nonlinear Optical Crystal BaGa₄Se₇. *Crystals* **2017**, *7*, 62. [\[CrossRef\]](#)
11. Yao, J.; Mei, D.; Bai, L. BaGa₄Se₇: A new congruent-melting IR nonlinear optical material. *Inorg. Chem.* **2010**, *49*, 9212–9216. [\[CrossRef\]](#) [\[PubMed\]](#)
12. Yelissev, A.P.; Lobanov, S.I.; Krinitsin, P.G.; Isaenko, L.I. The optical properties of the nonlinear crystal BaGa₄Se₇. *Opt. Mater.* **2019**, *99*, 109564. [\[CrossRef\]](#)
13. Kolker, D.B.; Kostyukova, N.Y.; Boyko, A.A. Widely tunable (2.6–10.4 μm) BaGa₄Se₇ optical parametric oscillator pumped by a Q-switched Nd:YLiF₄ laser. *J. Phys. Commun.* **2018**, *2*, 035–039. [\[CrossRef\]](#)
14. Perdew, J.P.; Burke, K.; Ernzerhof, M. Generalized gradient approximation made simple. *Phys. Rev. Lett.* **1996**, *77*, 3865. [\[CrossRef\]](#) [\[PubMed\]](#)
15. Perdew, J.P.; Ruzsinszky, A.; Csonka, G.I.; Vydrov, O.A.; Scuseria, G.E. Restoring the density-gradient expansion for exchange in solids and surfaces. *Phys. Rev. Lett.* **2008**, *100*, 136–406. [\[CrossRef\]](#)
16. Wu, Q.; Dai, R.; Zhang, L.; Wang, W.; Zhang, F.C.; Zhang, W.B. Theoretical study of a novel infrared nonlinear optical crystal of BaGa₄S₇. *J. Nanoelectron. Optoelectron.* **2020**, *15*, 1–11. [\[CrossRef\]](#)
17. Kresse, G.; Furthmüller, J. Efficiency of ab-initio total energy calculations for metals and semiconductors using a plane-wave basis set. *Comput. Mater. Sci.* **1996**, *6*, 15–50. [\[CrossRef\]](#)
18. Hammer, B.; Hansen, L.B.; Nørskov, J.K. Improved adsorption energetics within density-functional theory using revised Perdew-Burke-Ernzerhof functionals. *Phys. Rev. B* **1999**, *59*, 7413. [\[CrossRef\]](#)
19. Grimme, S. Semiempirical GGA-type density functional constructed with a long-range dispersion correction. *J. Comput. Chem.* **2006**, *27*, 1787–1799. [\[CrossRef\]](#)
20. Liu, N.N.; Song, R.B.; Sun, H.Y.; Du, D.W. First-principles calculation of electronic structure and thermodynamic properties of Mg₂Sn. *Acta Phys. Sin.* **2008**, *57*, 7145–7150.
21. Huang, K. (Ed.) *Solid Physic*; Higher Education Press: Beijing, China, 2002; p. 439.
22. Fang, R.C. (Ed.) *Solid State Pectroscopy*; University of Science and Technology of China Press: Hefei, China, 2001.
23. Shen, X.C. (Ed.) *Spectra and Optical Properties of Semiconductors*, 2nd ed.; Science Press: Beijing, China, 2002.
24. Yang, C.Y.; Zhang, R.; Zhang, L.M.; Ke, X.W. Electronic structure and optical properties of 0.5NdAlO₃-0.5CaTiO₃ from first-principles calculation. *Acta Phys. Sin.* **2012**, *61*, 077–702.
25. Feng, J.; Xiao, B.; Chen, J.C. Electronic and optical properties of CuInSe₂ from ab-initio calculations. *Acta Phys. Sin.* **2007**, *56*, 5990–5995. [\[CrossRef\]](#)
26. Li, X.Z.; Xie, Q.; Chen, Q.; Zhao, F.J.; Cui, D.M. The study on the electronic structure and optical properties of OsSi₂. *Acta Phys. Sin.* **2010**, *59*, 2016–2021.
27. Zhou, H.G.; Wen, X.W.; Fang, Z.X.; Li, Y.; Ding, K.N.; Huang, X.; Zhang, Y.F. Electronic structures and optical properties of AgGa(S_{1-x}Se_x)₂ solid solutions. *Chem. Phys.* **2013**, *29*, 920–928.
28. Wang, L.; Men, Y.B. Comparison study of CsLiB₆O₁₀ and β-BaB₂O₄ as nonlinear media for optical parametric oscillators. *Appl. Optics.* **2003**, *42*, 2720–2723. [\[CrossRef\]](#)
29. Chen, W.D.; Cousin, J. Continuous-wave mid-infrared laser sources based on difference frequency generation. *Comptes Rendus Phys.* **2007**, *8*, 1129–1150. [\[CrossRef\]](#)
30. Hazama, H.; Takatani, Y. Integrated ultraviolet and tunable mid-infrared laser source for analyses of protein. *Proc. Soc. Photo-Opt. Instrum. Eng.* **2007**, *6455*, 45507.